LES of flow over the NASA Common Research Model with near-wall modeling

By O. Lehmkuhl†, G. I. Park AND P. Moin

Large-eddy simulation (LES) with algebraic equilibrium wall model was used to study the NASA Common Research Model with the wing-body (WB) and wing-body-pylon-nacelle (WBPN) configurations at $\mathrm{Re} = 5{\cdot}10^6$ and $\mathrm{Ma} = 0.85$. Results initially obtained with coarse and medium grid resolutions show good agreement with available experimental data. Improvement of the LES solution on the coarse grid when a wall model is introduced is clearly demonstrated by comparison to the LES solution obtained with the no-slip wall boundary condition. Wall-modeled LES appears to significantly outperform the state-of-art RANS method at a comparable grid resolution in terms of predicting the global lift force.

1. Introduction

Reliable prediction of high Reynolds number flows in external aerodynamics has long been one of the primary aims in computational fluid dynamics (CFD). Modeling high-speed turbulent flows over complex geometries subjected to rapid variations in the strain and vorticity remains a challange this field. The Reynolds-averaged Navier-Stokes (RANS) techniques that account for the majority of current CFD analyses in the related industry have been of limited utility in the design cycle owing to the inaccuracy of turbulence models. RANS predictions of the flow regimes near the flight envelope become particularly less credible, because RANS models fail to predict flow separation that strongly affects the optimal aircraft performance (e.g., maximum lift) and its rapid loss (e.g., stall). LES avoids the pitfalls in RANS methodologies by resolving most of the energetic events in the flow directly, and modeling only the small-scale motions more amenable to universal modeling. However, the routine use of such external aerodynamics in resolved LES is rarely considered in currently, owing to the computational costs.

The boundary layer, among many other flow features, presents a modeling challenge owing to its multi-scale nature both in time and space. The behavior of the small structures in the inner layer has strong impact on the development of the outer layer and far-field regions. An accurate representation of dynamically important near-wall eddies (or their effect on the outer-layer solution) is required. As their size with respect to the boundary layer thickness diminishes rapidly with increasing Reynolds numbers and as standard subgrid models do not perform well on coarse grid resolution, resolved LES requires computational meshes with a quasi-DNS grid resolution. The cost of wall-resolved LES of high Reynolds number flows around airborne vehicles often exceeds the capacity of most powerful supercomputers to date, and therefore its use in industry is deemed infeasible.

Several approaches have been developed in recent years in order to broaden the application range of LES computations. These aim to model the turbulent momentum transport

† Technical University of Catalonia, Spain

from the inner layer to outer layer, instead of resolving the inner region directly. These strategies can be split into two categories: hybrid RANS-LES and wall stress methods. The main conceptual difference between the two methodologies is that in hybrid RANS-LES, the wall model is embedded in the turbulence model itself. The model returns a RANS-type turbulent viscosity in the near-wall regions while it switches to a LES subgrid type viscosity in the outer and far-field regions. By contrast, in wall shear stress methods, a LES model is solved down to the wall while an external wall model provides a wall-shear stress to the LES domain as an approximate boundary condition.

Such wall shear stress models require further validation and development in order to be used in real-life industry. The focus of the present research is to generate a first reference solution with equilibrium shear stress wall models in complex geometries, as a precursor to the adoption of wall-modeled LES (WMLES) by the external aerodynamics community. To this end, the NASA Common Research Model at $\mathrm{Re} = 5 \cdot 10^6$, $\mathrm{Ma} = 0.85$, and angle of attack $(\mathrm{AoA}) = 4^\circ$ is used as a numerical test of the Werner & Wengle (1993) algebraic equilibrium wall model. Here, Re denotes the Reynolds number based on the mean aerodynamic chord of the CRM wing and the ambient freestream velocity, and Ma denotes the freestream Mach number. Earlier work on this geometry (see the 5th and 6th Drag Prediction Workshops (DPW), https://aiaa-dpw.larc.nasa.gov/) has focused on RANS models. A large scattering of global-force prediction results from various RANS closures has been observed ($\Delta C_L = 0.043$) at the selected AoA. Hence, it is also of interest to see how well WMLES performs in this specific configuration compared to the state-of-art RANS technique.

2. Formulation and computational setup

The numerical platform used in the present study is the TermoFluids CFD code (Lehmkuhl *et al.* 2007). The code has been designed to run efficiently on high-end supercomputers. The parallelization of TermoFluids is based on a distributed memory model using the standard Message-Passing Interface (MPI). Very close attention has been paid on the parallelization of the linear solvers, because most of the simulation time is spent on solving the linear system derived from the discretization. A good scalability up to 131072 CPUs was obtained recently (Borrell *et al.* 2016) on Blue Gene/Q IBM supercomputers at Argonne Leadership Computing Facility (ALCF). This excellent parallel performance has allowed our group to win allocations for two Tier-0 research projects sponsored by PRACE, the institution that holds the largest supercomputers in Europe.

The code deploys finite volume (FV) techniques for discretization of the compressible Navier-Stokes equations on unstructured grids. The FV method provides a flexible framework to generate the computational domain comprised of structured, unstructured, or hybrid meshes. Although structured meshes provide additional accuracy from error cancellation when reconstructing numerical flux on the face out of the state variables stored in cell centroids, they impose severe restrictions on the distribution of cells. Often to many control volumes have to be placed in zones where no physically meaningful process is happening, in order to place a large enough number of control volumes in the regions of interest. On the other hand, unstructured meshing allows control volumes to be placed where it is necessary without increasing the number of cells in other regions. Additionally, local refinements, as well as generating structured subsets within an unstructured mesh, can be performed more easily.

To avoid artificial numerical dissipation that deteriorates the solution at small scales,

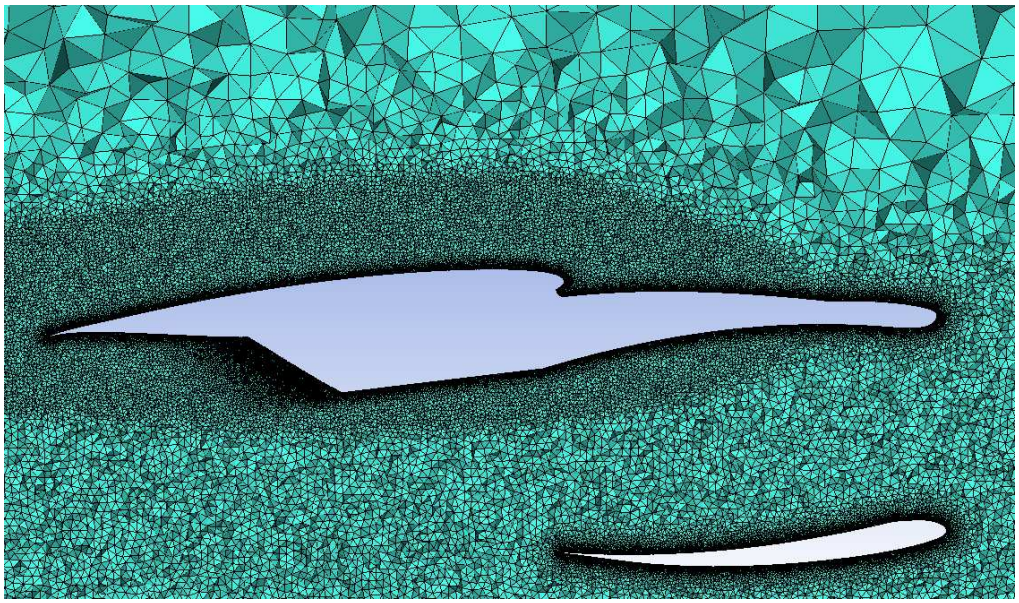

FIGURE 1. Mesh slice detail for the 103M CVs and WBNP configuration. A cross-section of the wing-pylon-nacelle at a constant spanwise coordinate on the wing is shown. The top geometry is the wing-pylon-nacelle combination, and the bottom one is the part of the nacelle. Flow is from right to left.

energy- and entropy-consistent schemes (Ducros *et al.* 2000) are employed for discretization of the convective terms. In the present simulations, a skew-symmetric scheme that switches to an advanced upwind-like method in the close vicinity of shock-waves is used, in order to introduce artificial viscosity selectively in the regions where it is mandatory (Pedro *et al.* 2016). Additionally, shock detection is carried out by means of the Larsson detector (Larsson *et al.* 2011). The upwind part of the hybrid method is a second-order TVD with a flux limiter. The subgrid-scale terms in the LES equation are closed with an unstructured version of the dynamic Smagorinsky model (Germano *et al.* 1991) proposed by Lehmkuhl (2012).

Given the high Reynolds number of the selected cases, wall modeling is essential to close the numerical setup. As the first step in this project, a standard algebraic equilibrium wall model was selected (Werner & Wengle 1993). As a follow up to the summer program activities, we plan to test a two-layer non-equilibrium model proposed by Park & Moin (2014) and the integral wall model proposed by Yang *et al.* (2015).

In light of the restrictions on time and on computational resources available in the Summer Program, two unstructured grids with different mesh resolution levels have been designed for both the WB and WBNP configurations. In both cases, following the 6th DPW recommendations, the wing deflections observed in the experiment have been introduced into the geometrical model. The coarse grids consist of 16M and 12M control volumes (CVs) for the WB and WBNP configurations, respectively, where fewer than 3 elements are used across the wing boundary layer. For the higher-resolution grids, 75M and 103M CVs are used. In this case, roughly 10 elements are located inside the wing boundary layer. In all cases, the mesh is constructed to be quasi-uniform in the wall-tangential directions with a smooth stretching in the normal directions (see Figure 1). Additionally, volumetric mesh density has been adjusted to capture only the largest scales

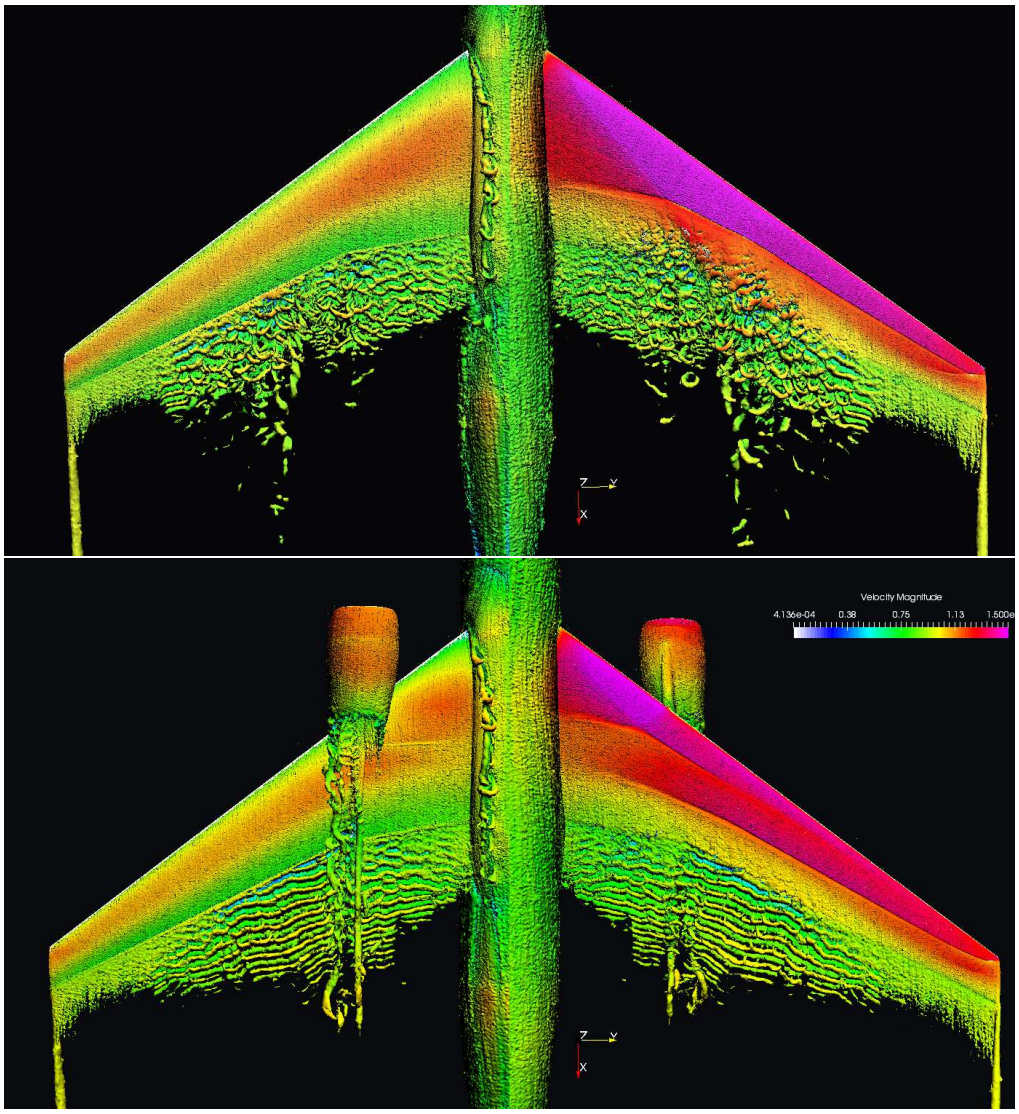

FIGURE 2. Q iso-isosurfaces colored by velocity magnitude, (top) WB configuration with 75M CV mesh and (bottom) WBNP configuration 103M CV mesh. The left and right halves of each figure show the pressure and suction sides of the wing, respectively.

of the flow. In the present study, 256 CPUs from the Certainty cluster and 996 CPUs from the Marenostrum Supercomputer were used for the calculations with the coarse and finer meshes, respectively. The largest simulation required approximately 140K CPU hours.

3. Results and discussion

In Figure 2, iso-surfaces of the second invariant Q of the velocity-gradient tensor colored by the velocity magnitude are depicted. A transient longitudinal structure is generated in the bottom junction between the fuselage and the wing; this structure is present in both configurations. In addition, the tip vortex is also observed with similar topology

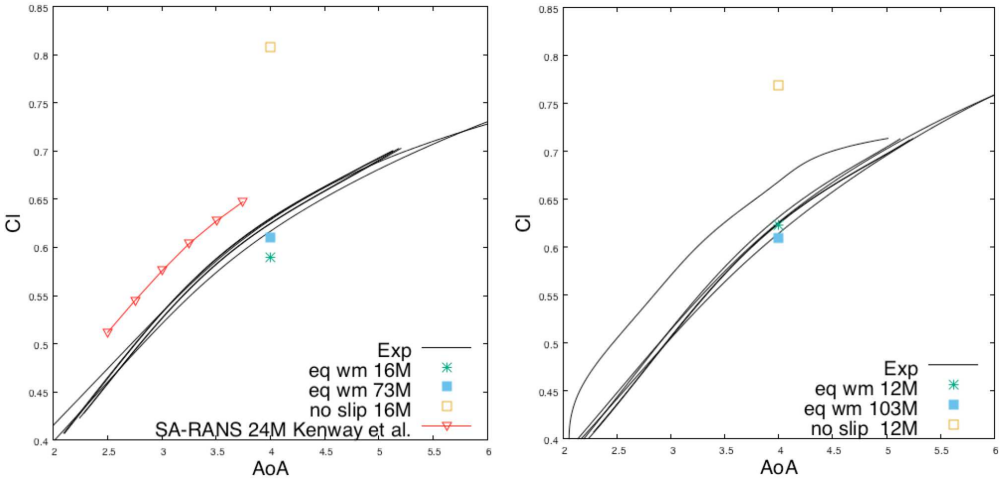

FIGURE 3. Averaged total lift coefficient: WMLES vs experimental data, (left) WB configuration and (right) WBNP configuration.

in both cases. However, large differences in the shock-induced separation in the trailing edge of the wing are observed. For the WB configuration, the separation has enough energy to produce vortex dislocation of the wing wake. These vortex dislocations can be seen around the mid-span, producing some hairpin-like vortices. However, in the WBNP configuration, the increase momentum generated presumably by the nacelle results in a delayed shock-induced separation with less energy. This separation does not have enough energy to break the quasi two-dimensional vortex structures behind the wing. Finally, due to the wing, pylon and nacelle interaction, several transient vortical structures are shed from this region (see Figure 2 bottom). These structures are further mixed with the wing wake in the near-wake region, but they do not change the overall wake configuration.

In Figure 3, the total lift for both configurations is compared to the experimental data. A RANS prediction from the 6th DPW is also included for the WB configuration (courtesy of Kenway *et al.* (2016)). For the sake of completeness, we also present the results obtained with the no-slip wall boundary condition and the coarse meshes . As can be seen in the figure, the no-slip LES results are completely off the experimental results. By contrast, the results from the WMLES are in fair agreement with the experimental data, even on the coarse meshes. WMLES prediction of the global lift force appears to be significantly more accurate than the prediction obtained with the state-of-art Spalart-Allmaras one-equation RANS model. While the RANS data in Figure 3 was obtained with a relatively smaller number of CVs, the fact that only less than 2% change in the drag coefficient was observed in the RANS grid convergence study using approximately 10M to 100M CVs implies that the converged lift coefficient from the RANS would still remain far from the experimental data. Comparing the WB and WBNP configurations, the nacelle seems to have limited impact on the overall lift coefficient at the angle of attack considered in the present study.

For a more detailed analysis of the results of the WMLES on both configurations, the local distribution of the pressure coefficient (C_p) at stations η =0.397, 0.502, and 0.727 is depicted in Figure 4. Here, η denotes the normalized spanwise coordinate deployed in the experiment, where $\eta = 0$ and 1 corresponds to the WB junction and the wing tip, respectively. In both configurations, the coarse WMLESs fail to reproduce the shock

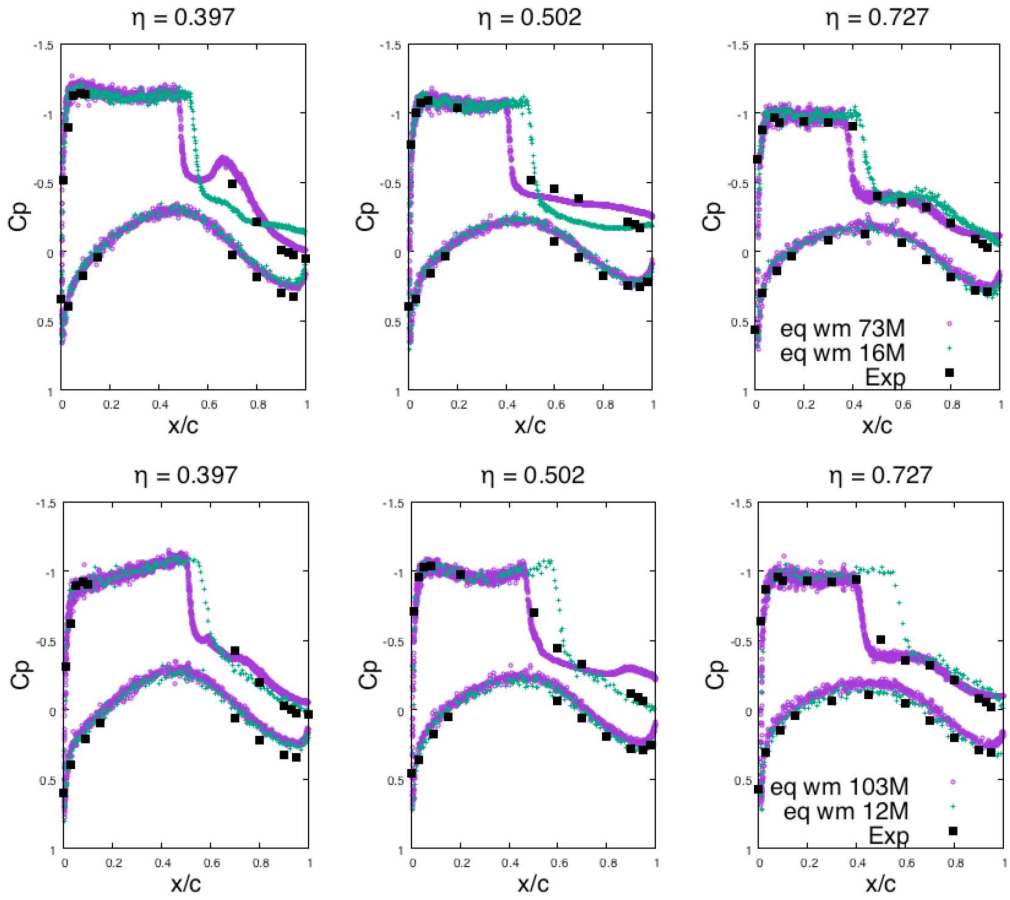

FIGURE 4. Local C_p distributions at different spanwise sections: WMLES vs experimental data, (top) WB configuration, and (bottom) WBNP configuration.

location, resulting in a delayed detachment. However, with the finer meshes (73M CVs for the WB case and 103M CVs for the WBNP case), WMLES results are in good agreement with the experiment. As anticipated from the instantaneous Q iso-surface plots, the nacelle produces a slight delay in the shock location which is more evident in the outboard plot ($\eta = 0.727$). Moreover, for the inboard section ($\eta = 0.397$), WMLES is capable of reproducing the increase in the C_p observed in the WB configuration experiments after the shock. However, with the current grid resolution, it is not possible to analyze in more detail wether this pressure recovery after the shock on the suction side is responsible for the change in the wake flow configuration observed in the instantaneous plots.

4. Conclusions

The NASA Common Research Model with the wing-body and wing-body-pylon-nacelle configurations (Re = 5M, Ma = 0.85) have been studied for the first time with LES employing an algebraic equilibrium model. The time-averaged total lift forces obtained with coarse and medium resolutions (16/12M and 75/103M control volumes for the WB and WBNP configurations, respectively) show good agreement with the available experimen-

tal data. In addition, the need for wall modeling at coarse grid resolution has been clearly demonstrated. Simulation results show that the inclusion of the nacelle produces a delay in the shock location which in turn induces a lesser energetic separation. However, the local C_p comparison between the WMLES and experimental data shows a slight discrepancy in the shock location. Additional mesh refinement studies are needed to investigate this aspect in more detail.

Acknowledgments

The authors acknowledge the use of computational resources from the CTR Certainty cluster awarded by the National Science Foundation.

REFERENCES

Vassberg, J. C., DeHaan, M. A., Rivers, M. B. & Wahls, R. A. 2008 Development of a common research model for applied CFD validation studies. *AIAA Paper* 2008-6919.

Lehmkuhl, O., Perez-Segarra, C.D., Borrell, R., Soria, M. & Oliva, A. 2007 TermoFluids: A new parallel unstructured CFD code for the simulation of turbulent industrial problems on low PC Clusters. *Parallel Comput. Fluid Dyn.* 275–282

Werner, H. & Wengle, H. 1993 Large-eddy simulation of turbulent flow over and around a cube in a plate channel, *Turbulent Shear Flows* **8**, 155–168.

Borrell, R., Chiva, J., Lehmkuhl, O., Oyarzun, G. & Oliva, A. 2016 Optimising the TermoFluids CFD code for petascale simulations. *Int. J. Comput. Fluid Dyn.*, **30**, 425–430.

Ducros, F., Laporte, F., Souleres, T., Moinat, P. & Caruelle, B. 2000 High-order fluxes for conservative skew-symmetric-like schemes in structured meshes: application to compressible flows. *J Comput. Phys.* **161**, 114–139.

Germano, M., Piomelli, U., Moin, P., & Cabot, W. H. 1991 A dynamic subgrid scale eddy viscosity model. *Phys. Fluids* **3**, 1760-1765.

Lehmkuhl, O. 2012 *Numerical resolution of turbulent flows on complex geometries.* PhD Thesis, Technical University of Catalonia, Spain.

Larsson, J., Vicquelin, R. & Bermejo-Moreno, I. 2011 Large eddy simulations of the HyShot II scramjet. *Annual Research Briefs.*, Center for Turbulence Research, Stanford University, pp 63–74.

Park, G. I. & Moin, P. 2014 An improved dynamic non-equilibrium wall-model for large eddy simulation, *Phys. Fluids.* **26**, 015108.

Pedro, JB., Vidal, AB., Lehmkuhl, O., Segarra, CD. & Oliva, A. 2016 On the extension of LES methods from incompressible to compressible turbulent flows with application to turbulent channel flow. *J. Phys.: Conf. Series.***745**, 032047

Yang, X.I.A., Sadique, J., Mittal, R., & Meneveau, C. 2015 Integral wall model for large eddy simulations of wall-bounded turbulent flows. *Phys. Fluids.* **27**, 025112.

Kenway, G. K. W., Secco, N., & Martins, J. R. R. A. 2016 Drag prediction workshop VI: SUMad Results.